Article

Not peer-reviewed version

Inorganic Polyphosphate Promotes Colorectal Cancer Growth via TRPM8 Receptor Signaling Pathway

Valentina Arrè *, Francesco Balestra, Rosanna Scialpi, Francesco Dituri, Rossella Donghia, Sergio Coletta, Dolores Stabile, Antonia Bianco, Leonardo Vincenti, Salvatore Fedele, Chen Shen, Giuseppe Pettinato, Maria Principia Scavo, Gianluigi Giannelli, Roberto Negro *

Posted Date: 10 September 2024

doi: 10.20944/preprints202409.0739.v1

Keywords: Colorectal cancer; inorganic polyphosphate; TRPM8 receptor; organoids; ccnb1; proliferation

Article

Inorganic Polyphosphate Promotes Colorectal Cancer Growth via TRPM8 Receptor Signaling Pathway

Valentina Arrè [1,*], Francesco Balestra [1], Rosanna Scialpi [1], Francesco Dituri [1], Rossella Donghia [2], Sergio Coletta [3], Dolores Stabile [3], Antonia Bianco [3], Leonardo Vincenti [4], Salvatore Fedele [4], Chen Shen [5], Giuseppe Pettinato [6], Maria Principia Scavo [1,‡], Gianluigi Giannelli [7,‡] and Roberto Negro [1,*,‡]

[1] Personalized Medicine Laboratory, National Institute of Gastroenterology "S. de Bellis", IRCCS Research Hospital, Via Turi 27, Castellana Grotte, 70013, Bari, Italy
[2] Data Science, National Institute of Gastroenterology "S. de Bellis", IRCCS Research Hospital, Via Turi 27, Castellana Grotte, 70013, Bari, Italy
[3] Core facility Biobank, National Institute of Gastroenterology "S. de Bellis", IRCCS Research Hospital, Via Turi 27, Castellana Grotte, 70013, Bari, Italy
[4] Department of Surgery Sciences, Unit of Surgery, National Institute of Gastroenterology "S. de Bellis", IRCCS Research Hospital, Via Turi 27, Castellana Grotte, 70013, Bari, Italy
[5] Division of Infectious Diseases, Washington University School in Medicine in St. Louis, 660 S Euclid Ave, St. Louis, MO 63110, USA
[6] Division of Gastroenterology, Department of Medicine, Beth Israel Deaconess Medical Center, Harvard Medical School, 330 Brookline Avenue, Boston, MA 02215, USA
[7] Scientific Direction, National Institute of Gastroenterology, "S. de Bellis", IRCCS Research Hospital, Via Turi 27, Castellana Grotte, 70013, Bari, Italy
* Correspondence: valentina.arre@irccsdebellis.it; roberto.negro@irccsdebellis.it
‡ co-senior authors contributed equally to this work.

Simple Summary: The Inorganic polyphosphate, a molecule composed of a few to several hundred orthophosphates, is involved in disparate pathological processes, including cancer development and progression. In this study, by analyzing biopsies derived from 50 subjects carrying colorectal cancer, collected by the Histopathology Unit of IRCCS "S. de Bellis", we showed a significant discrepancy of the level of the inorganic polyphosphate between tumoral and peritumoral counterpart, with the former displaying higher concentration. Moreover, by employing in-vitro and ex-vivo approaches, we enlightened an involvement of the inorganic polyphosphate in colorectal cancer cell proliferation. Additionally, we identified the calcium channel TRPM8 as the inorganic polyphosphate receptor responsible to propagate the signal downstream and, ultimately, enhance the expression of proliferative markers. Thus, our results recognize the inorganic polyphosphate as novel pivotal biomarker linked with colorectal cancer growth.

Abstract: Colorectal cancer (CRC) is characterized by a pro-inflammatory microenvironment and features high energy supply molecules that assure tumor growth. A still underestimated macromolecule is the Inorganic Polyphosphate (iPolyP), a high-energy linear polymer that is ubiquitous in all forms of life. Made up of hundreds of repeated orthophosphate units, iPolyP is essential for a wide variety of functions in mammalian cells, including the regulation of proliferative signaling pathways. Some evidence has suggested its involvement in carcinogenesis, although more studies need to be pursued. In this study, we tested the role of iPolyP on CRC proliferation, using in-vitro and ex-vivo approaches, in order to evaluate its effect on tumor growth. We found that iPolyP is significantly increased in tumor tissues compared to the corresponding peritumoral counterparts. In addition, iPolyP signaling occurs through the TRPM8 receptor, promoting CRC cell proliferation. Pharmacological inhibition of TRPM8 or RNA interference experiments showed that the involvement of TRPM8 is essential, greater than that of the other two known iPolyP receptors, P2Y1 and RAGE. The presence of iPolyP drives cancer cells towards the mitotic phase of the cell cycle by enhancing the expression of *ccnb1*, which encodes for the Cyclin B protein. In-vitro 2D and 3D data reflected the ex-vivo results, obtained by the generation of CRC-derived organoids, which increased in size. These results indicate that iPolyP may be considered a novel and unexpected early biomarker supporting colorectal cancer cell proliferation.

 doi:10.20944/preprints202409.0739.v1

Keywords: colorectal cancer; inorganic polyphosphate; TRPM8 receptor; organoids; ccnb1; proliferation

1. Introduction

Colorectal cancer (CRC) remains the third most deadly cancer diagnosed worldwide, and shows an increasing incidence in both developing and developed countries [1]. Individuals bearing CRC display backgrounds that cover a wide range of genetic or epigenetic alterations [2,3]. Sporadic or induced mutations in the CRC scenario often fall within a discrete set of tumor suppressor genes, like adenomatous polyposis coli (APC), SMAD4 family member (SMAD4), or those traditionally involved in the regulation of cell proliferation and cell cycle, like p53 [4]. In addition, mutations in oncogenes, particularly concerning genes such as Kristen rat sarcoma virus (KRAS), phosphatidylinositol 4,5-bisphosphate 3-kinase catalytic subunit-α (PIK3CA), or b-raf proto-oncogene (BRAF), confer hyperproliferative traits to intestinal epithelial cells, that promote a genetic hypermutability scenario [5]. Lifestyle, environmental mutagens or, more recently, dysbiotic metabolites, are emerging as pivotal ingredients in CRC onset and development [6], although mechanistically, a number of queries remain unaddressed and novel potential candidates need to be disclosed. Food additive inorganic polyphosphate (iPolyP) is a biological polymer, structurally composed by from 3 to over 1000 orthophosphates linked together by ATP-like bonds [7], can spontaneously arise from non-living matter or be enzymatically produced by living organisms, including bacteria and eukaryotes [8]. While synthesis and degradation of iPolyP in bacterial cells has been well-studied, the corresponding metabolic pathways in the eukaryotic counterpart are still poorly understood [9]. Mammalian iPolyP has been found in nuclei, mitochondria, lysosomes, platelets dense granules, mast cells- and basophils-derived granules [10–13]. iPolyP architecture makes it an obvious participant of energy metabolism. It is, in fact, nowadays considered a phosphate donor for ATP synthesis [14]. Thus, considered an optimal source of energy, emerging literature has started to associate iPolyP to various pathophysiological processes over the past few decades, including inflammation-driven diseases [15–20], tumorigenesis [9], tumor metastasis [21,22] and cellular proliferation [23,24]. It has been shown that iPolyP mediates cellular proliferation by selectively upregulating the mechanistic target of rapamycin (mTOR) phosphorylation at Ser2481 [23]. Three binding receptors have been identified for iPolyP: namely the advanced glycosylation end-product specific receptor (RAGE), purinergic receptor P2Y1 and transient receptor potential cation channel subfamily M (melastatin) member 8 (TRPM8) [25,26]. Preliminary evidences lighted up a novel pathway involving iPolyP/RAGE receptor linked to Wingless-related integration site (Wnt)/β-catenin signaling axis, of crucial importance for the regulation of major pathophysiological processes in tumor cells [27]. However, besides slight evidences about iPolyP-mediated cell proliferation, not many studies have yet reported associations between iPolyP, its receptor and cancer [28], perhaps due to difficulties in iPolyP quantification and lack of comparative data for neoplastic and corresponding normal counterpart. Parallelly, recent literature has reported an overexpression of TRPM8 receptor in CRC specimens, which correlates with poorer survival [29]. TRPM8 belong to the transient receptor potential (TRP) cation channel superfamily, subfamily melastatin (M), member 8 (TRPM8), also known as the cold and menthol receptor 1 (CMR1) [30]. However, its clinical relevance remains largely fragmented. In our study we tested the amount of iPolyP in tumoral and peritumoral tissues of enrolled colorectal cancer subjects, showing a significant discrepancy. Moreover, we determined the role of TRPM8 receptor as mediator of iPolyP signaling, which, ultimately, leads to the activation of proliferative marker in CRC. Overall, these findings might add iPolyP to the list of early biomarkers of CRC, together with DNA, RNA and proteins, shown to prolong the overall survival of patients [31], thus potentially paving the way for the development of novel anticancer agents as supplement to conventional chemotherapy.

2. Materials and Methods

 doi:10.20944/preprints202409.0739.v1

2.1. Patients' Samples

In this retrospective study, samples derived from 50 patients with CRC, who were candidates for surgical treatment, were studied. Patients provided written informed consent to the collection of blood samples for biomarker analysis under Prot. No. 397/C.E. of 16/09/2020 of the Local Ethics Committee "Gabriella Serio" IRCCS Istituto Tumori "Giovanni Paolo II", Bari, Italy. Biopsy tissue specimens were provided by the Histopathology Unit of IRCCS "S. de Bellis". The analyses were performed by comparing two different sections of histological sample from the same patients, so as to identify a healthy portion (Normal or Peritumoral) and a diseased portion (Pathological or Tumoral).

2.2. Tissue Preparation

Patients (Pt) tissues, subdivided into two counterparts, Peritumoral (PT) and Tumoral (T), were tested for the amount of iPolyP, by fluorometric assay, and for the level of PCNA and TRPM8 by immunoblotting. Tissues were lysed using a tissue homogenizer (TissueLyser II), (QIAGEN, Hilden, Germany; Cat. no. 85300) in Buffer III/Poly P Extraction Buffer, for iPolyP detection, described in detail in the Inorganic polyphosphate detection assay section, or in T-PER™ Tissue Protein Extraction Reagent supplemented with Halt™ Protease and Phosphatase Inhibitor Single-Use Cocktail, EDTA-Free (100X) for protein analysis, described in the immunoblotting section.

2.3. Inorganic Polyphosphate Detection Assay

Inorganic polyphosphate was detected in tumoral and peritumoral tissues, using the Inorganic Polyphosphate Assay Kit (Fluorometric), (Abcam, Cambridge Biomedical Campus, Cambridge, U.K.; Cat. no: ab284528) following relative manufacturer's recommendations. Briefly, homogenized tissues were centrifuged at 10,000 x g for 15 minutes at 4°C and the clear supernatant was collected and treated with RNAse Positive Control/RNase, DNase and Proteinase K. 100 µL of the stock polyphosphate standard/iPolyP standard solution was mixed with 900 µL of water to prepare 10 µM polyphosphate standard/iPolyP standard solution used to assay and plot the polyphosphate standard curve. To test 5 µL of each sample in triplicate, 96-wells plates were prepared, adjusting the volume of each well to 50 µL using Polyphosphate Assay Buffer/iPolyP Assay Buffer. Reaction mix at 50 µL including 47 µL of Polyphosphate Assay Buffer and 3 µL of Polyphosphate Dye, was added to each well, including standards and samples. The plates were incubated for 10 minutes at room temperature and the fluorescence of all wells was measured at Ex/Em = 415/550 nm at room temperature in endpoint mode. Calculation of the amount of inorganic polyphosphate was performed using the following equation: Amount of iPolyP (pmol/mg) = A x D / W x Vt / Va, where: A = Amount of iPolyP was calculated from the polyphosphate standard/iPolyP standard curve (pmol), D = Sample dilution factor (D = 1, for undiluted samples), W = Weight of the tissue used (in mg) or protein amount as determined by the protein assay (mg), Vt = Total sample volume, Va = Volume of sample measured in the well. Protein amount (in mg) was determined using Bio-Rad (Bio-Rad Laboratories, Hercules, California, U.S.A.; Cat. no: Hercules, California, U.S.A.; Cat. no: 5000006EDU) protein assay dye reagent.

2.4. Cell Culture and Reagents

Human colorectal adenocarcinoma Caco-2 and SW620 cells were purchased from the American Tissue Culture Collection (ATCC, Manassas, Virginia, U.S.A.; Cat. no. HTB-37 and CCL-227, respectively). Human Colonic Epithelial Cells 1 transduced with CDK4 and Telomerase HCEC-1CT cells were purchased from Evercyte GmbH (Vienna, Austria; Cat. no. CkHT-039-0229). Caco-2 and SW620 cells were grown in Dulbecco's Modified Eagle's medium (DMEM), (Thermo Fisher Scientific, Waltham, Massachusetts, U.S.A.; Cat. no: 11965092), supplemented with 10% fetal bovine serum (Thermo Fisher Scientific, Waltham, Massachusetts, U.S.A.; Cat. no: A5256701), 1 mM Sodium Pyruvate (Thermo Fisher Scientific, Waltham, Massachusetts, U.S.A.; Cat. no: 11360039), 25 mM HEPES (Thermo Fisher Scientific, Waltham, Massachusetts, U.S.A.; Cat. no: 15630056) and 100 U/mL

 doi:10.20944/preprints202409.0739.v1

Antibiotic-Antimycotic (Thermo Fisher Scientific, Waltham, Massachusetts, U.S.A.; Cat. no: 15240062). Human Colonic Epithelial Cells 1 transduced with CDK4 and Telomerase (HCEC-1CT) were grown in ColoUp medium ready to use (Evercyte GmbH, Vienna, Austria; Cat. no: MHT-039), supplemented with 100 U/mL Antibiotic-Antimycotic. All cell lines were maintained in a humidified atmosphere at 37°C with 5% CO_2. Cells were passaged and medium was changed every other day.

2.5. Cellular Treatments

HCEC-1CT, Caco-2 and SW-620 cell lines were seeded into 6-well plates (Corning, New York, New York, U.S.A.; Cat. no. 3516) at a density of 0.5 x 10^6 cells/well in 2 mL of complete cell culture medium. Seeded cells were treated with 0.5 μM of sodium phosphate glass (iPolyP) (Sigma-Aldrich, St. Louis, Missouri, U.S.A.; Cat. no: S4379-500mg), or with 10 μM of TRPM8 receptor inhibitor N-(3-Aminopropyl)-2-[(3-methylphenyl)methoxy]-N-(2-thienylmethyl)benzamide hydrochloride (AMTB), (Santa Cruz Biotechnology, Dallas, Texas, U.S.A.; Cat. no: 926023-82-7), or in combination for 72 hours. Dimethyl sulfoxide (DMSO), (Sigma-Aldrich, St. Louis, Missouri, U.S.A.; Cat. no. D8418-100mL) was added to the control cells. Pharmacological inhibition of the iPolyP/TRPM8 axis was performed by adding AMTB to the HCEC-1CT, Caco-2 and SW620 cell lines. Pharmacological inhibition of the P2Y1 receptor was performed with Adenosine 2′,5′-diphosphate sodium salt (Santa Cruz Biotechnology, Dallas, Texas, U.S.A.; Cat. no: SC-214495); RAGE receptor inhibition was performed with (Abcam, Cambridge Biomedical Campus, Cambridge, U.K.; Cat. no. ab235552). Cells were centrifuged at 1100 rpm for 5 minutes at 4°C and washed with 1X of sterile Dulbecco's phosphate buffered saline 1 (1X DPBS) (Thermo Fisher Scientific, Waltham, Massachusetts, U.S.A.; Cat. no. 14190-094) twice. Dried pellets were frozen at - 80°C or resuspended and lysed in 200 μL of T-PER™ Tissue Protein Extraction Reagent (Thermo Fisher Scientific, Waltham, Massachusetts, U.S.A.; Cat. no: 78510) supplemented with Halt™ Protease and Phosphatase Inhibitor Single-Use Cocktail, EDTA-Free (100X) (Thermo Fisher Scientific, Waltham, Massachusetts, U.S.A.; Cat. no. 78443) for immunoblotting analysis.

2.6. Immunoblotting

Both tissue and cellular lysates were incubated on ice for 30 minutes and vortexed every 10 minutes. Samples were then centrifuged at 16,000 rpm at 4°C for 20 minutes to clarify and precipitate insoluble debris. Total extracted proteins were assayed to measure concentrations using the Bio-Rad protein assay dye reagent concentrate (Bio-Rad Laboratories, Hercules, California, U.S.A.; Cat. No: 5000006EDU). Then, proteins were mixed with 4 x Laemmli Sample Buffer (Bio-Rad Laboratories, Hercules, California, U.S.A.; Cat. No: 1610747) and 10% of β-mercaptoethanol (Sigma-Aldrich, St. Louis, Missouri, U.S.A.; Cat. No: M6250-100mL) and denatured at 95°C for 5 minutes. 25 μg of proteins were loaded onto precast polyacrylamide 4-20% gels (Bio-Rad Laboratories, Hercules, California, U.S.A.; Cat. No: 4568094), subsequently blotted on a polyvinylidene fluoride (PVDF) membrane (Bio-Rad Laboratories, Hercules, California, U.S.A.; Cat. No: 1704156) using the trans-blot turbo transfer system (Bio-Rad Laboratories, Hercules, California, U.S.A.; Cat. No. 1704150). Membranes were blocked using Pierce™ Protein-Free Blocking Buffer (Thermo Fisher Scientific, Waltham, Massachusetts, U.S.A.; Cat. No: 37571) for 1 hour and stained overnight with primary antibodies. The next day membranes were washed three times with 1X of Tris Buffered saline (1X TBS), (Bio-Rad Laboratories, Hercules, California, U.S.A.; Cat. No: 1706435 diluted in ddH_2O to reach 1X)/TWEEN20 (Sigma-Aldrich, St. Louis, Missouri, U.S.A.; Cat. No: P9416-100mL) incubated for 1 hour with the respective horseradish peroxidase-conjugated secondary antibodies. Proteins were detected using the Clarity Max Western ECL Substrate (Bio-Rad Laboratories, Hercules, California, U.S.A.; Cat. No: 1705062) and the signals were obtained using the Chemidoc MP Imaging System (Bio-Rad Laboratories, Hercules, California, U.S.A.; Cat. No. 1708280). The following primary antibodies were used: anti-PCNA, 1:1000 (Santa Cruz Biotechnology, Dallas, Texas, U.S.A.; Cat. No. SC-56); anti-TRPM8, 1:1000 (Thermo Fisher Scientific, Waltham, Massachusetts, U.S.A.; Cat. No. MA5-35474); anti-GAPDH, 1:1000 (Santa Cruz Biotechnology, Dallas, Texas, U.S.A.; Cat. No. SC-47724); anti-β-Actin, 1:1000 (Cell Signaling Technology, Danvers, Massachusetts, U.S.A.; Cat. No.

 doi:10.20944/preprints202409.0739.v1

4970S); anti-P2Y1-R, 1:1000 (Abcam, Cambridge Biomedical Campus, Cambridge, U.K.; Cat. No. ab168918); anti-RAGE-R, 1:1000 (Abcam, Cambridge Biomedical Campus, Cambridge, U.K.; Cat. No. ab216329). GAPDH and β-Actin were used as loading controls. The following secondary antibodies were employed: Anti-rabbit IgG, HRP-linked Antibody, 1:2000 (Cell Signaling Technology, Danvers, Massachusetts, U.S.A.; Cat. no. 7074S); Goat anti-Mouse IgG (H+L)-HRP Conjugate (Bio-Rad Laboratories, Hercules, California, U.S.A.; Cat. no: 1706516).

2.7. Knockdown of TRPM8 with siRNA

For TRPM8-knockout experiments using siRNA, HCEC-1CT, Caco-2 and SW620 were electrophored with two TRPM8 Silencer siRNAs (Thermo Fisher Scientific, Cat. no. 4392420, ID: S35489 and ID: S35490, respectively) or with Silencer siRNA Negative Control (Thermo Fisher Scientific, Cat. no. 4390843). Electroporation was performed using the Neon™ NxT Electroporation System (Thermo Fisher Scientific, Cat. no. NEON1SK), according to the manufacturer's recommendations.

2.8. Crystal Violet Assay

HCEC-1CT, Caco-2 and SW620 cells were seeded into 96-well plates (Corning, New York, New York, U.S.A.; Cat. No. 3599) at a density of 2 x 10^3 cells/well in 100 µL of complete medium and left overnight to allow complete attachment. The next day (considered t = 0 hour), the medium was removed and replaced with 100 µL of fresh serum-free medium to allow cell cycle synchronization. Seeded cells in triplicate wells were treated and maintained in the different conditions: 0.5 µM of iPolyP, or 10 µM of AMTB, or both in combination, for 96 hours. Controls were cells treated with DMSO. After 96 hours, cells were fixed by adding 100 µL/well of 4% paraformaldehyde (PFA), (Sigma-Aldrich, St. Louis, Missouri, U.S.A.; Cat. no. P6148-500G), pH 7.6 at room temperature for 30 minutes to the medium (obtaining 2% PFA final concentration). Each well was subsequently stained with 0.02% of crystal violet solution (Sigma-Aldrich, St. Louis, Missouri, U.S.A.; Cat. no. HT90132-1L) for 10 minutes and washed with cold water to eliminate surplus staining. Images were collected with a Nikon Ti2 inverted laser-scanning confocal microscope equipped with a 10X objective (0.25 numerical aperture), as described in the immunofluorescence and confocal microscopy section, in bright-field and analyzed with NIS-Elements software (version 5.11.01) and ImageJ2 (version 2.14.0/1.54f) before complete solubilization. Finally, cell-bound crystal violet staining was redissolved in aqueous solution containing 1% sodium dodecyl sulfate (SDS), (Sigma-Aldrich, St. Louis, Missouri, U.S.A.; Cat. no. L3771-100G) at room temperature for 30 minutes and the absorbance was measured at λ = 595 nm with the iMark™ Microplate Absorbance Reader (Bio-Rad Laboratories, Hercules, California, U.S.A.; Cat. No. 168-1130).

2.9. Immunofluorescence Microscopy

2 x 10^5/mL cells were grown in 35-mm petri dishes, no. 1.5 coverglass (MatTek, Ashland, Massachusetts, U.S.A.; Cat. no. P35G-1.5-14-C). Fixative, permeabilization, and blocking buffers were prepared in 1X DPBS. Cells were fixed with 4% PFA for 30 minutes at room temperature and then washed twice using 1X DPBS. Permeabilization was performed for 5 minutes at room temperature using 0.15% Triton X-100 (in 1X DPBS). Washing was performed to remove permeabilization buffer. Cells were then blocked for 1 hour at room temperature using blocking buffer (3% bovine serum albumin (BSA), (Sigma-Aldrich, St. Louis, Missouri, U.S.A.; Cat. no. A7030-100G)/1X DPBS). Cells were incubated with primary antibody overnight. Nuclei were stained using PureBlu DAPI (Bio-Rad Laboratories, Hercules, California, U.S.A.; Cat. no. 1351303). Extensive washing steps were performed to remove unbound stain. Anti-Ki67 (ready-to-use, Abcam, Cambridge Biomedical Campus, Cambridge, U.K.; Cat. no. ab16667) was used as primary antibody. Images were collected with a Nikon Ti2 inverted laser-scanning confocal microscope equipped with Plan Apo 20X (0.75 numerical aperture) in bright-field and analyzed with NIS-Elements software (version 5.11.01) and ImageJ2 (version 2.14.0/1.54f). All fluorescence images were collected with a confocal Yokogawa

 doi:10.20944/preprints202409.0739.v1

spinning-disk on a Nikon Ti inverted microscope equipped with Plan Fluor 20X (0.75 numerical aperture) lens; bright-field micrographs relative to CRC organoids were acquired with Plan Fluor 60X (0.85 numerical aperture); bright-field micrographs relative to spheroids were acquired with Plan Fluor 40X (0.60 numerical aperture) and 20X. Images were acquired with a Hamamatsu ORCA ER cooled CCD camera controlled with NIS-Elements software (version 5.11.01). Images were collected using an exposure time of 700 milliseconds. Gamma, brightness, and contrast were adjusted on displayed images (identically for comparative image sets) using NIS-Elements software (version 5.11.01). The Perfect Focus System was kept running for continuous maintenance of focus. DMEM without phenol red (Thermo Fisher Scientific, Waltham, Massachusetts, U.S.A.; Cat. no. 21063-045) was used during image acquisition.

2.10. CRC Tumor Organoids

CRC specimens from surgically resected tumor tissue were washed three times with 1X DPBS and digested with collagenase/hyaluronidase mixture (Stemcell Technologies, Cat. no. 07912), diluted in HBSS solution (with $CaCl_2$ and $MgCl_2$, Thermo Fisher Scientific, Waltham, Massachusetts, U.S.A.; Cat. no. 14025-050) for 5 hours under gentle rocking at 37°C. A single cell suspension was obtained and cells were embedded in matrigel matrix basement membrane (Corning, New York, New York, U.S.A.; Cat. no. 356231), and cultured in IntestiCult-SF (ICT-SF) medium (Stemcell Technologies, Vancouver, British Columbia, Canada; Cat. no. 100-0340) medium diluted 1:2 in Advanced DMEM/F-12 (Thermo Fisher Scientific, Waltham, Massachusetts, U.S.A.; Cat. no. 12634-010), supplemented with N-2 (Thermo Fisher Scientific, Waltham, Massachusetts, U.S.A.; Cat. no. 17502-048), B27 supplement (Thermo Fisher Scientific, Waltham, Massachusetts, U.S.A.; Cat. no. 12587-010), 0.01% bovine serum albumin, antibiotic/antimycotic, and HEPES. Medium was renewed every two days until the organoids were fully developed (7-10 days). Mature organoids were split using TrypLE Select dissociation agent (Thermo Fisher Scientific, Waltham, Massachusetts, U.S.A.; Cat. no. A12177-01) according to [32] and the suspended cells obtained were re-cultured at a lower density in matrigel.

2.11. CRC Tumor Organoid Growth Test

Mature CRC tumor organoids were split to obtain single cell suspensions. Cells were counted and 2,000 cells were embedded in 40 µL of matrigel (with a matrigel density of 65%) in 96-well plates, cultured in ICT-SF medium, and allowed to grow for 10 days in the presence or absence of iPolyP at a concentration of 0.5 µM. Medium and iPolyP were replaced every 2 days. At the end point of the experiment, microscopic images of organoids were acquired in bright-field with the Nikon Confocal Microscope Eclipse Ti2. The growth rate of organoids was determined using CellTiter 96 AQueous One Solution Cell Proliferation Assay (Promega Corporation, Fitchburg, Wisconsin, U.S.A.; Cat. no. G3580), according to the manufacturer's recommendations.

2.12. Cell Lines-Derived Spheroids

1 x 10^3 of Caco-2, SW620 and HCEC-1CT cells were seeded into 3D low attachment 96-well cell culture plates (Corning, New York, New York, U.S.A.; Cat. no. 4520) to obtain 3D cell line spheroids with 100 µL of growth medium in each well. Cells were kept in culture in the above-mentioned conditions. After seeding, all cell lines were treated with iPolyP and/or AMTB, while untreated cells were used as controls (untreated, UT). Spheroid cultures were observed at 24, and 96 hours and maintained in a humidified incubator set to 37°C and 5% CO_2. After 96 hours, UT and treated cells were fixed with a 4% paraformaldehyde solution in 1X PBS and used for microscopy analysis.

2.13. Gene Expression Analysis by Real-Time Quantitative Reverse Transcription PCR

Caco-2 cells were seeded into 6-well plates at a density of 0.5 x 10^6 cells/well in 2 mL of complete cell culture medium. Seeded cells were treated with 0.5 µM of iPolyP, for 72 hours; untreated cells were used as control. Caco-2 cells were seeded into 6-well plates at a density of 0.5 x 10^6 cells/well in

 doi:10.20944/preprints202409.0739.v1

2 mL of complete cell culture medium. Seeded cells were treated with 0.5 μM of iPolyP, for 72 hours; untreated cells were used as control. Untreated cells were used as control. RNA extraction was performed from frozen cell pellets using RNeasy Mini Kit (QIAGEN, Hilden, Germany; Cat. no: 74104) according to the manufacturer's recommendations. The RNA concentration was measured using a NanoDrop 2000c (Thermo Fisher Scientific, Waltham, Massachusetts, U.S.A.; Cat. no. ND-2000) and 2 μg total RNA was reverse transcribed to cDNA using a High-Capacity cDNA Reverse Transcription Kit (Thermo Fisher Scientific, Waltham, Massachusetts, U.S.A.; Cat. no 4368814) following the relative protocol. Reactions were induced using the iTaq Universal SYBR Green Supermix (Bio-Rad Laboratories, Hercules, California, U.S.A.; Cat. no: 1725124) and the validated human primers purchased from Bio-Rad (Hercules, California, U.S.A.), with the following assay ID numbers: CCNA1, qHsaCID0008934; CCNB1, qHsaCID0010571; CCND1, qHsaCID0013833; GAPDH, qHsaCED0038674. Real-Time PCR analysis was performed with CFX96 Touch Deep Well Real-Time PCR Detection System (Bio-Rad Laboratories, Hercules, California, U.S.A.; Cat. no. 3600037) and experiments were conducted for three times in triplicate. Relative expression was calculated using the $2^{-\Delta\Delta Ct}$ method.

2.14. Cell Cycle Assay

Caco-2 and SW620 cells were seeded into 24-well plates (Corning, New York, New York, U.S.A.; Cat. no. 3524) at a density of 2 x 10^4 cells/well in 100 μL of complete medium and left overnight to allow complete attachment. The following day the medium was replaced with fresh serum-free medium to allow cell cycle synchronization. Cells were treated with 0.5 μM of iPolyP, or with 10 μM AMTB hydrochloride, or both in combination for 72 hours. Controls were cells treated with DMSO. After treatments 150 μL of cell-clock dye, from the Biocolor Cell-Clock™ Cell Cycle Assay (Ilex Life Science, Candler, North Carolina, U.S.A.; Cat. no. C1000) kit, were added to the center of each well and incubated for 1 hour at 37°C, according to the manufacturer's recommendations. Culture medium added with reagent was softly discarded and replaced with 200 μL of fresh medium. Micrographs of live cells were acquired using a Nikon Confocal Microscope Eclipse Ti2 in bright field equipped with a Plan Fluor 20X (0.75 numerical aperture) lens, and all experiments were conducted in triplicate. The calculation of phase percentages was obtained by analysis made with ImageJ2 software. The Redox dye used in this test is uptaken by live cells and the outcome is a color-defined cell cycle stage; each color was associated to cells in G0-G1 (yellow staining), S (green staining), G2 and M (dark green/blue phases).

2.15. Statistical Analysis

Patients' characteristics are reported as Mean and Standard Deviation (M ± SD), and as frequencies and percentages (%) for categorical. To compare iPolyP values between groups, Mann–Whitney rank test was used for continuous variables. Spearman rank correlation coefficient was used to test the strength and direction of associations between iPolyP and TRPM8/PCNA. When testing the null hypothesis of no association, the two-tailed probability level of error was set at 0.05. All statistical computations were made using StataCorp. (2021) Stata Statistical Software: Release 17 (StataCorp LLC, College Station, Texas, U.S.A.), while RStudio ("Chocolate Cosmos" Release, Posit PBC, Massachusetts, U.S.A.) was used for the plots.

3. Results

3.1. Human Colorectal Cancer Tissue Displays Enhanced Levels of iPolyP That Are Correlated with the Proliferation Marker PCNA

To estimate the iPolyP levels in patients with colorectal cancer (CRC), we recruited 50 patients undergoing surgery. Males (m) had a higher prevalence of CRC (52.00%) than females (f) (48.00%) at an average mean age of 71.53 ± 11.19 years. Tumor-Nodes-Metastasis (TNM) and grading classification of each subject is shown in Table 1. From each subject we collected the peritumoral portion and tumoral counterpart to perform iPolyP level detection. Intriguingly, the concentration of

 doi:10.20944/preprints202409.0739.v1

iPolyP was higher in tumoral tissue than in the peritumoral section, with a statistically significant difference (373097.70 ± 210216.20 pmol/mg vs 166102.70 ± 124618.80 pmol/mg, respectively), suggesting a putative role of iPolyP in promoting the tumorigenicity of CRC (Figure 1A). Moreover, in the same analyzed samples, tumoral tissue exhibited elevated levels of the proliferating cell nuclear antigen (PCNA) protein, a well-known marker of DNA replication and cellular proliferation, when compared to the matched peritumoral tissue (Figure 2A). In addition, a strong positive correlation between iPolyP and PCNA expression was found ($\varrho = 0.44$, **** $p < 0.0001$) (Figure 2B), which further suggests a synergistic pro-tumorigenic contribution of iPolyP to CRC development.

Table 1. Patients index with age at the time of the surgery, sex, stage Tumor, Node, Metastasis (TNM) and grading.

Patient	Age	Sex	Diagnosis	TNM	Grading
1	58	f	CRC	T1N0MX	G3
2	58	m	CRC	T1N0MX	G2
3	58	f	CRC	T1N0MX	G2
4	81	f	CRC	T2N0MX	G3
5	72	m	CRC	T2N0MX	G2
6	78	f	CRC	T2N0MX	G3
7	76	m	CRC	T2N0MX	G3
8	82	m	CRC	T2N0MX	G2
9	85	m	CRC	T2N0MX	G2
10	73	f	CRC	T2N0MX	G3
11	82	f	CRC	T2N0MX	G2
12	81	m	CRC	T2N1aMX	G2
13	70	m	CRC	T2N1aMX	G3
14	60	f	CRC	T2N1aM1	G3
15	71	m	CRC	T3N0MX	G2
16	75	m	CRC	T3N0MX	G2
17	59	f	CRC	T3N0MX	G3

 doi:10.20944/preprints202409.0739.v1

18	69	m	CRC	T3N0MX	G3
19	89	m	CRC	T3N0MX	G3
20	72	f	CRC	T3N0MX	G3
21	59	f	CRC	T3N0MX	G3
22	77	f	CRC	T3N0MX	G3
23	70	m	CRC	T3N0MX	G2
24	65	m	CRC	T3N0MX	G3
25	43	f	CRC	T3N0MX	G2
26	76	m	CRC	T3N0MX	G2
27	65	f	CRC	T3N0MX	G2
28	74	m	CRC	T3N0MX	G2
29	69	f	CRC	T3N0MX	G3
30	71	f	CRC	T3N0MX	G2
31	70	f	CRC	T3N0M1b	G2
32	88	m	CRC	T3N1aMX	G2
33	74	m	CRC	T3N1aMX	G2
34	80	f	CRC	T3N1aMX	G3
35	74	m	CRC	T3N1aMX	G3
36	70	f	CRC	T3N1aMX	G3
37	67	f	CRC	T3N1aMX	G3
38	78	m	CRC	T3N1bMX	G2/G3
39	79	m	CRC	T3N1bMX	G3
40	77	m	CRC	T3N1bMX	G3

 doi:10.20944/preprints202409.0739.v1

41	83	m	CRC	T3N2aMX	G3
42	76	m	CRC	T4aN0MX	G3
43	56	m	CRC	T4aN1MX	G3
44	35	m	CRC	T4aN1bMX	G3
45	86	m	CRC	T4aN2bMX	G2
46	93	f	CRC	T4aN2bM1c	G3
47	81	f	CRC	T4bN0MX	G2
48	71	f	CRC	T4bN0MX	G2
49	53	f	CRC	T4bN0MX	G2
50	74	f	CRC	T4bN0MX	G2

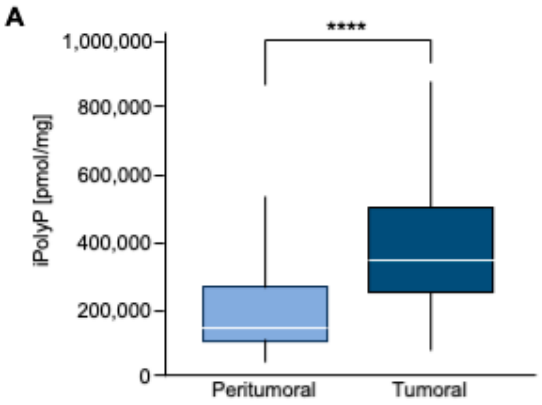

Figure 1. A. Box Plot of iPolyP distribution, stratified by Peritumoral or Tumoral patients. Statistical difference was found (median value of 373097.70 ± 210216.20 pmol/mg for tumoral tissue vs 166102.70 ± 124618.80 pmol/mg for the peritumoral counterpart, **** $p < 0.0001$). Analysis was performed by Mann–Whitney rank test.

 doi:10.20944/preprints202409.0739.v1

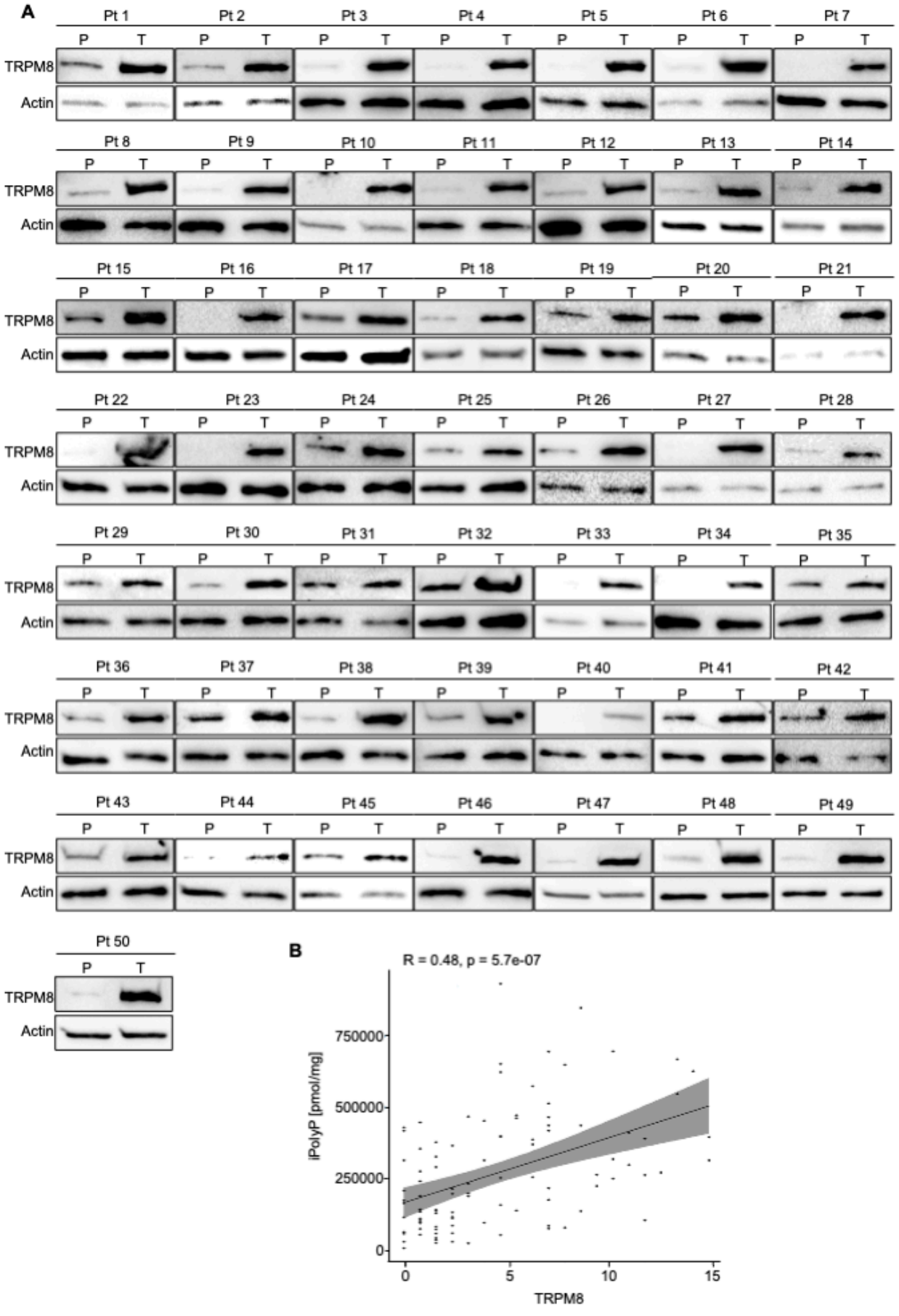

 doi:10.20944/preprints202409.0739.v1

Figure 2. CRC displays high level of PCNA. **A**. Cellular extracts from 50 human biopsies, where Tumoral sample (T) was plotted against the Peritumoral (P) counterpart of the same patient (Pt), were analyzed by immunoblotting for PCNA expression level. Actin was used as loading control for the normalization. **B**. Spearman correlation between iPolyP and PCNA in total cohort denoting a strong positive correlation (**** $p < 0.0001$). Fold changes versus Peritumoral (P), normalized to 1.

3.2. The iPolyP-TRPM8 Signaling Axis Sustains Colorectal Cancer Cell Proliferation

To determine whether iPolyP has pro-neoplastic properties and, if so, which receptor-binding partner signals to the colorectal cancer milieu, we initially screened biopsies from the same cohort of enrolled subjects, for the P2Y1 receptor (P2Y1-R), RAGE receptor (RAGE-R) and TRPM8 channel receptor, all well-recognized iPolyP receptors. Among these, only TRPM8 appeared to be overexpressed in the tumoral fraction compared with the peritumoral one (Figure 3A) in all samples, while the P2Y1-R and RAGE-R levels were not different (Supplementary Figure S1 A,B). Moreover, similarly to PCNA, we found a strong positive correlation between the concentration of iPolyP within the tumoral tissues and TRPM8 receptor expression ($\varrho = 0.48$, **** $p < 0.0001$), (Figure 3B), supporting the hypothesis that iPolyP may primarily transduce through the TRPM8 receptor in the CRC context. Following these findings, we firstly explored whether the presence of iPolyP could somehow encourage the proliferation of colorectal cancer cells by interacting with the TRPM8 receptor. With an in vitro approach, we demonstrated that the administration of iPolyP induces the expression of PCNA in Caco-2 (Figure 4A) and in SW620 (Supplementary Figure S2A), non-metastatic and metastatic colorectal cancer cell lines, respectively, without altering the TRPM8 levels (Figure 4A). Surprisingly, no detectable effect of iPolyP was observed at PCNA level in HCEC-1CT cells, the cytogenetically normal and nontumorigenic colon-derived cell line (Supplementary Figure S3A). Following pharmacological inhibition or genetic abrogation of the TRPM8 receptor we could revert PCNA expression to levels comparable to those observed in the untreated samples, in both the colorectal cancer cell lines examined (Figure 4A, Supplementary Figure S2A), while no difference was observed in HCEC-1CT cells upon iPolyP challenge (Supplementary Figure S3A). Direct evidence of iPolyP-TRPM8 axis-mediated cellular proliferation was obtained with crystal violet staining, a quantitative assay that discriminates live versus dead cells based on the DNA intercalating dye, proportional to the number of adherent cells. After 96 hours, iPolyP revealed a marked propensity to promote Caco-2 and SW620 proliferation. Furthermore, as expected, by antagonizing or knocking down the TRPM8 receptor, we flattened the proliferation rate (Figure 4B,C and Supplementary Figure S2B,C). This significant highly proliferative phenotype is not discernible in HCEC-1CT cells upon iPolyP treatment, whose division rate remains unaltered (Supplementary Figure S3B,C). iPolyP does not seem to influence the expression levels of the P2Y1 and RAGE receptors, neither in HCEC-1CT nor in Caco-2 or in SW620 cells (Supplementary Figure S4A,B), thus excluding a positive feedback mechanism mediated by iPolyP underpinning the molecular regulation of its receptors. Proliferation assays performed on Caco-2 and SW620 with the P2Y1 or RAGE inhibitor demonstrated that iPolyP mainly triggers colorectal cancer cell expansion by binding to TRPM8, as hindrance of these pathways did not affect the proliferation induced by iPolyP (Supplementary Figure S4C,D). To corroborate the proliferative propensity of iPolyP we performed fluorescence microscopy experiments targeting Antigen Kiel 67, known as Ki-67, a second common marker for proliferation, in our model cell lines, whose outcome revealed PCNA alterations. In particular, upon iPolyP administration, Caco-2 and SW620 cells, but not HCEC-1CT, displayed an enhanced level of Ki-67, which was suppressed following TRPM8 inhibition or when silenced (Supplementary Figure S5A,B). Moreover, SW620 cells showed self-organization into spheroids, whose morphology appeared enlarged in the presence of iPolyP. All together, these data deliver an important take-home message regarding the capability of iPolyP to promote colorectal cancer cell growth by engaging the TRPM8 receptor.

 doi:10.20944/preprints202409.0739.v1

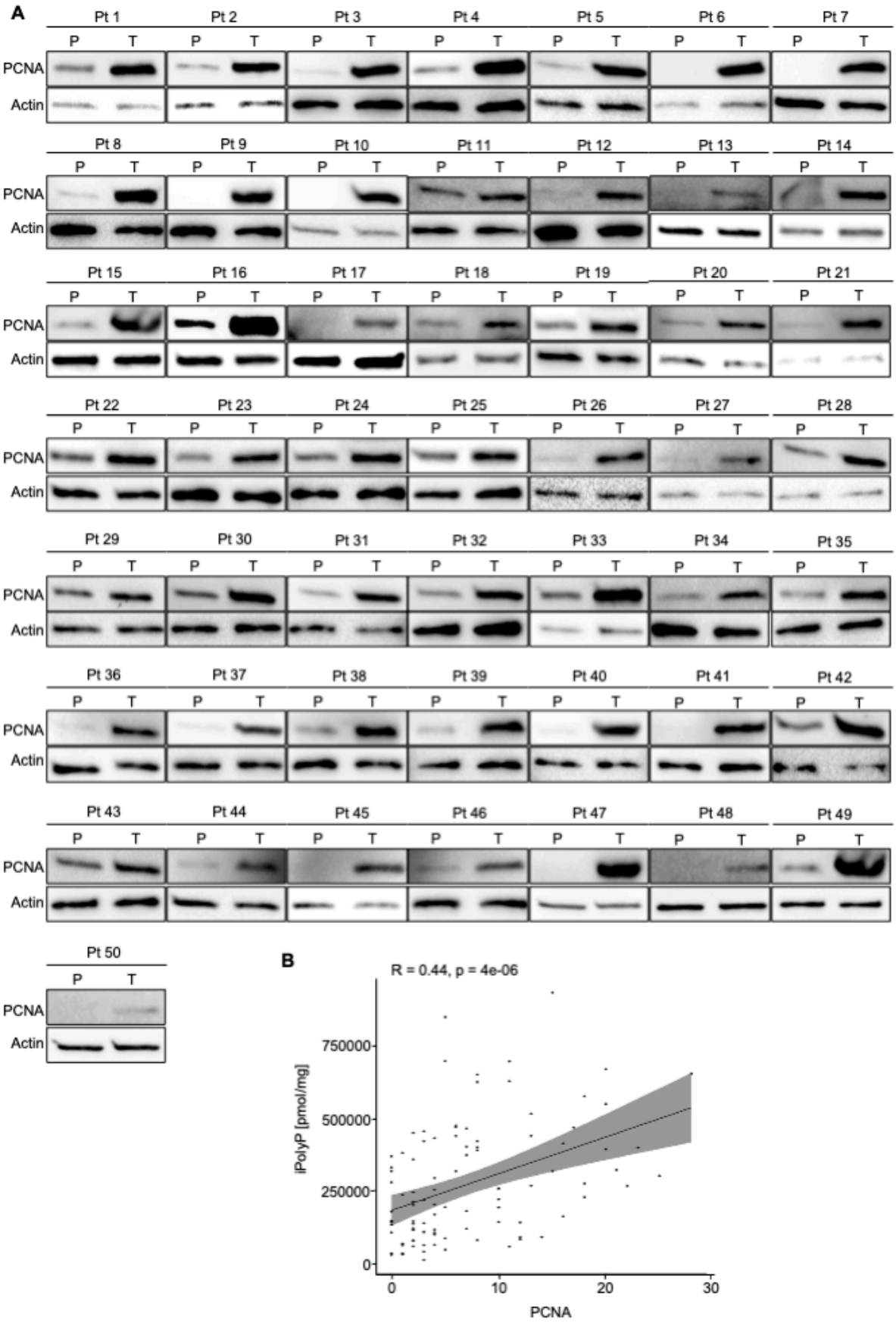

Figure 3. CRC displays high level of TRPM8 receptor. **A**. Cellular extracts from 50 human biopsies, where Tumoral sample (T) was plotted against the Peritumoral (P) counterpart of the same patient (Pt), were analyzed by immunoblotting for TRPM8 expression level. Actin was used as loading

 doi:10.20944/preprints202409.0739.v1

control for the normalization. **B**. Spearman correlation between iPolyP and TRPM8 in total cohort denoting a strong positive correlation (**** $p < 0.0001$). Fold changes versus Peritumoral (P), normalized to 1.

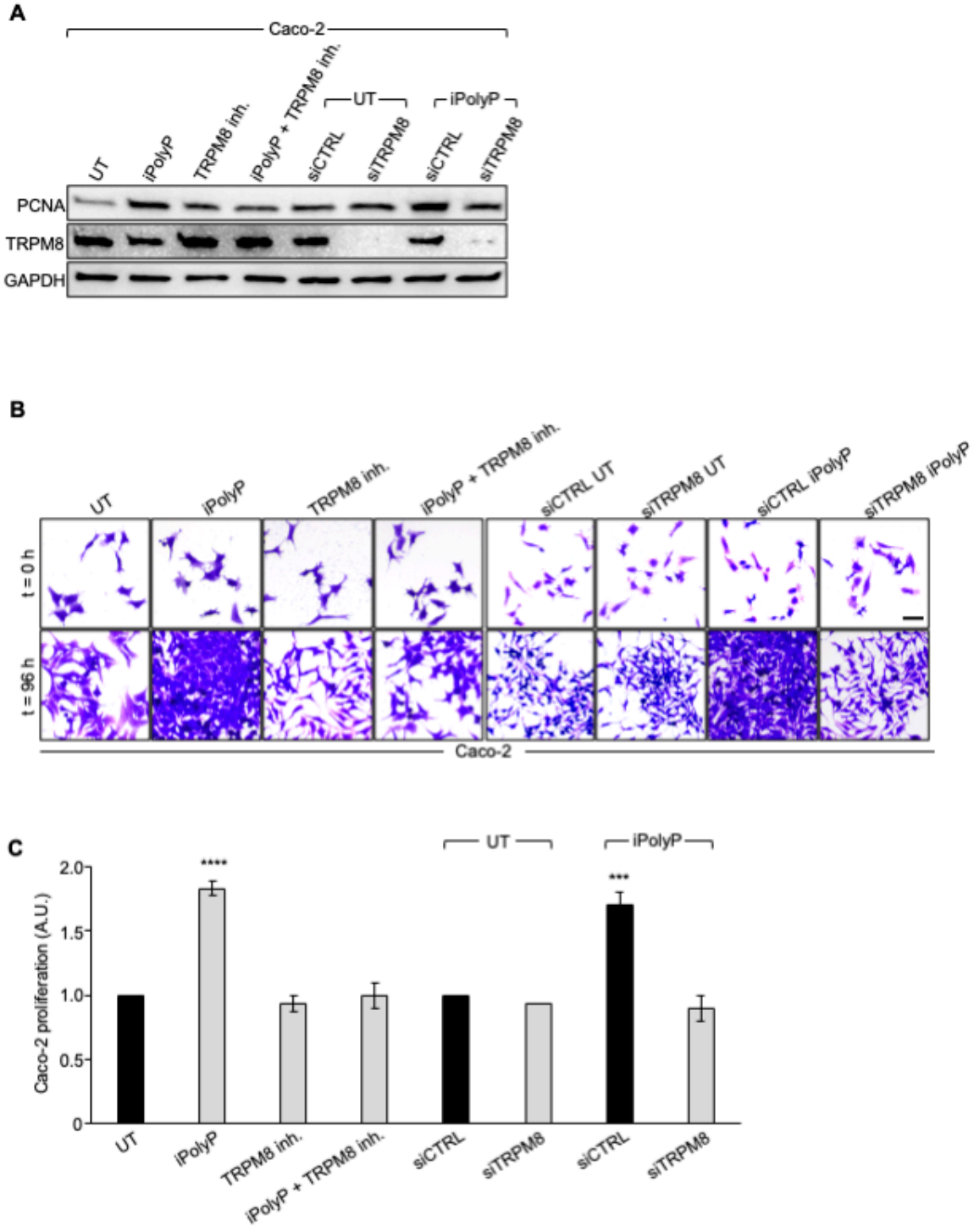

Figure 4. iPolyP enhances PCNA expression and promotes Caco-2 colorectal cancer proliferation. **A**. Cellular extracts from WT and siRNA-mediated TRPM8 knockdown Caco-2 cell lines were analyzed by immunoblotting for PCNA expression level. GAPDH was used as loading control. **B**. Representative micrographs of the crystal violet assay performed on WT and siRNA-mediated TRPM8 knockdown Caco-2 cell lines upon treatment for 96 h with iPolyP, TRPM8 inhibitor or both. Scale bar 10 μm. Images are representative of three independent experiments. **C**. Statistical analysis

 doi:10.20944/preprints202409.0739.v1

of the crystal violet assay by Student's t-test, respectively for panel C, (*** $p < 0.001$ and **** $p < 0.0001$). Fold changes versus control, untreated (UT), normalized to 1. Data are presented as mean ± SD for triplicate wells from three independent experiments.

3.3. iPolyP Encourages CRC Patient-Derived Organoids Growth and Caco-2- and SW620 Cells-Derived Spheroids Formation

Based on the above findings, we recapitulated the proliferative task of iPolyP with tests of CRC patient-derived organoids growth. We generated organoids from two CRC subjects and incubated them with iPolyP. As shown in Figure 5 panel A-B, the growth rate of the organoids in the presence of iPolyP was significantly higher than in those left untreated, for both independent experiments (Figure 5A,B). Moreover, these data reflected the evidence observed with Caco-2- and SW620 cells-derived spheroids; in particular, after 96 hours of incubation with iPolyP, the diameter of the spheroids was double than the untreated ones. The presence of the TRPM8 inhibitor abrogated the proliferative effect due to iPolyP. Finally, we could appreciate no change in HCEC-1CT cells (Figure 5C,D), confirming our conclusions regarding the role of iPolyP in CRC.

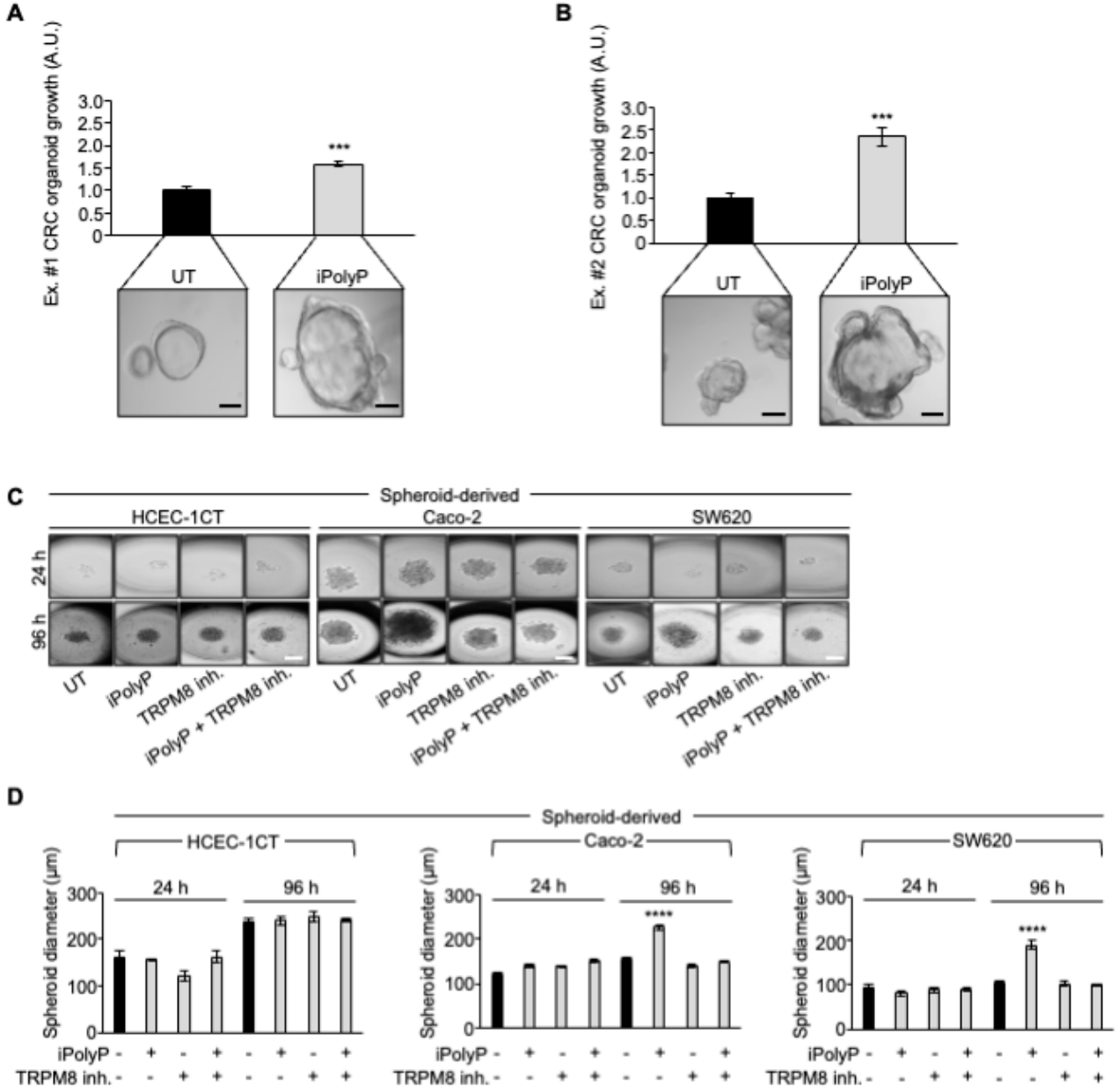

 doi:10.20944/preprints202409.0739.v1

Figure 5. iPolyP promotes colorectal cancer patient-derived organoid and Caco-2- and SW620-derived 3D spheroids. **A**, **B**. Two independent experiments of CRC patient's-derived organoids, assessed by light microscopy, in the absence (UT) or incubated for 10 days in the presence of iPolyP. Scale bar 100 μm. Fold changes versus control, untreated (UT), normalized to 1. Statistical analysis performed by Student's t-test (*** $p < 0.001$). **C**. Representative bright-field images of 24 h- and 96 h-induced spheroid formation derived from HCEC-1CT, Caco-2 and SW620 cell line, respectively, upon treatment with iPolyP, TRPM8 inhibitor or both for 96 h. Scale bar 100 μm. Images are representative of three independent experiments. **D**. Quantification relative to panel **C**. Fold changes versus control, untreated (UT). Statistical analysis performed by Student's t-test (**** $p < 0.0001$). Data are presented as mean ± SD for triplicate wells from three independent experiments.

3.4. iPolyP Induces ccnb1 Expression in the Caco-2 Cell Line and Drives the Cells into M Phase via the TRPM8 Receptor

To further explore the molecular mechanism by which inorganic polyphosphate drives the expansion of colorectal cancer cells, we performed real-time quantitative reverse transcription PCR experiments on Caco-2 cells-derived RNA, 72 hours post iPolyP treatment, probing genes involved in different phases of the cells cycle. Although we noticed a considerable increase, in terms of number of copies of transcripts related to genes like *ccnd1* (cyclin D1) and *ccna1* (cyclin A1), mainly involved in the G1 and S/G2 phases, respectively, a significant signal amplification was observed for the *ccnb1* transcript, which codes for the mitotic protein cyclin B, a master regulator of the G2/M phase (Figure 6A). Figure 6B summarizes the most relevant cyclins linked to different phases of the cell cycle. To make a cellular interpretation of the gene expression data we performed a "cell-clock" cell cycle assay on Caco-2 and SW620 cells exposed to iPolyP for 72 hours. This assay consists of live-cell detection employed to monitor the four major phases of the mammalian cell cycle through a redox dye. Following dye uptake, a distinct color change occurs within cells, denoting the specific G1, S, G2 and M phases of the cycle. In detail, it turns yellow in G1, green in S/G2 and blue in M phase. A significantly high percentage of blue-colored cells was spotted, following iPolyP administration, compared to the control sample, the latter being comparable to the TRPM8 inhibitor- or iPolyP + TRPM8 inhibitor-treated cells (Figure 6C-D). Overall, these data strengthen our interpretation of a pro-tumorigenic role of iPolyP in colorectal cancer cells.

Preprints.org (www.preprints.org) | NOT PEER-REVIEWED | Posted: 10 September 2024 doi:10.20944/preprints202409.0739.v1

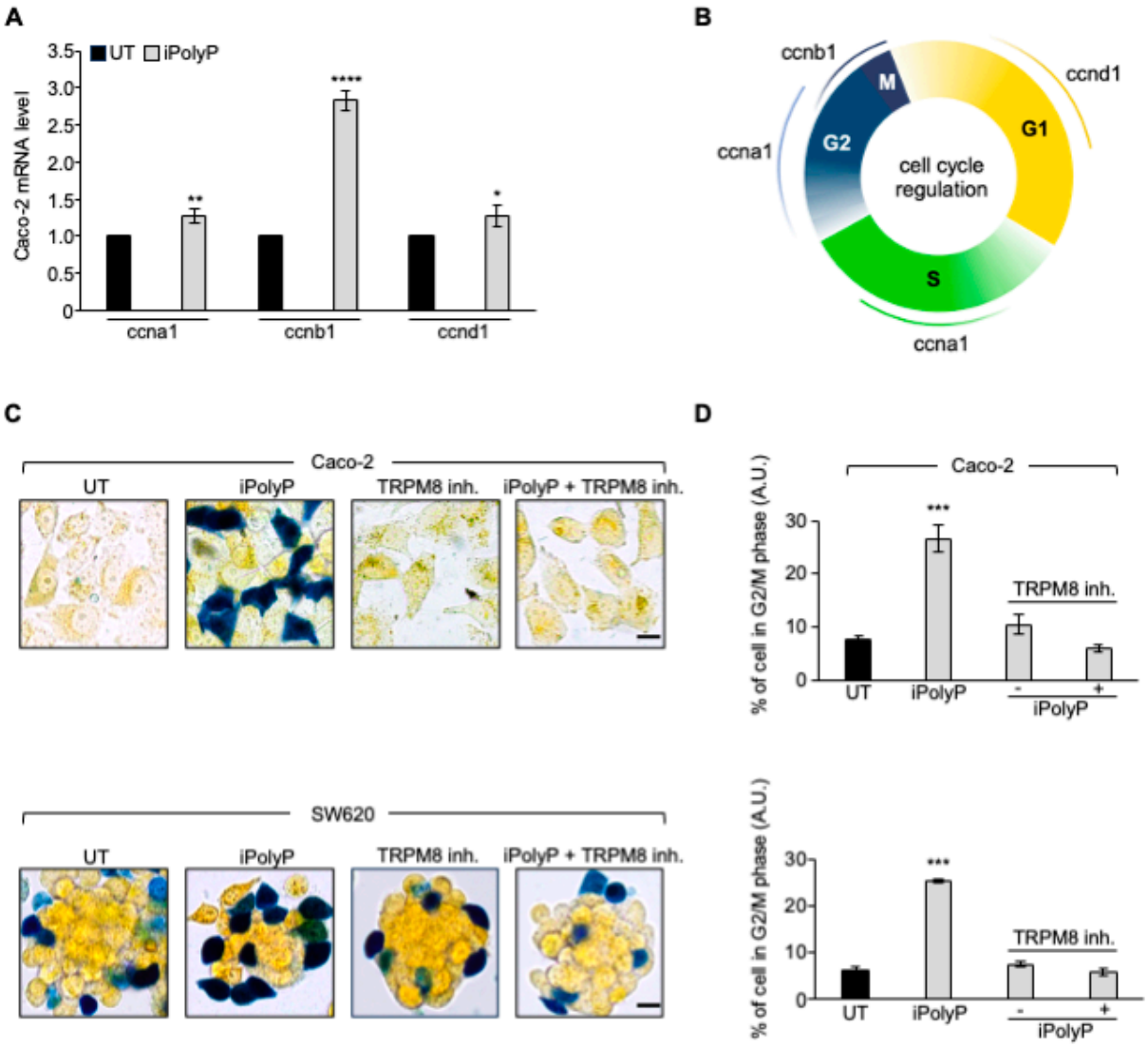

Figure 6. iPolyP drives cells into G2/M phase. **A**. Real-Time PCR on iPolyP-treated Caco-2 cell line for 72 h on cyclins implicated in difference phases of the cell cycle; untreated, UT, samples were normalized to 1. **B**. Sketch representing cyclins-dependent cell cycle regulation consisting of Gap 1 (G1), synthesis (S), Gap 2 (G2), and mitosis (M). Figure was created with BioRender. **C**. Representative micrographs of the cell cycle assay on Caco-2 (upper panel) and SW620 (lower panel) cell line treated for 72 h with iPolyP, TRPM8 inhibitor or both. Scale bar = 10 μm. Images are representative of three independent experiments. **D**. Percentage of cells in G2/M phase. Statistical analysis performed by Student's t-test (*** $p < 0.001$). Fold changes versus control, untreated (UT). Data are presented as mean ± SD for triplicate wells from three independent experiments.

4. Discussion

Despite the enormous efforts made striving towards the development of new therapeutical strategies targeting the molecular complexity discernible in colorectal cancer, CRC remains one of the deadliest human neoplasms [33]. The CRC elusiveness is primarily due to the interplay between advanced age, environmental and lifestyle factors, mammalian- and microbiota-derived metabolites and genetic alterations, underlying each stage of tumorigenesis [34,35], which limit effective CRC-specific therapy [36]. Cancer cell metabolism thrives best in a hypoxic environment and relies on alternative energy sources to survive and proliferate [37]. The linear polymer composed of several up to hundreds of phosphate residues, named inorganic polyphosphate, fits the role of energy supplier well, with its phosphoanhydride ATP-like bonds [38]. Not surprisingly, in fact, in vitro, an involvement of iPolyP in cancer cell proliferation and tumor progression has been recently proposed,

 doi:10.20944/preprints202409.0739.v1

and demonstrated [22], although the evidence is still minor, perhaps due to the difficulty in visualizing this macromolecule in experimental conditions. Enzymatically synthesized iPolyP has two known sources, bacterial and human. In bacteria, iPolyP ranges from 100 to 1,000 units thanks to the high processivity of the enzyme polyphosphate kinase 1 (*ppk1*), which uses ATP as substrate [39–41]. Human-derived iPolyP shows an average of ~60-100 phosphate residues, and no known kinase has so far been linked [42–44]. The different number of orthophosphate residues might affect the proliferative, pro-inflammatory and pro-tumorigenic tasks of iPolyP. Moreover, it is largely unknown whether iPolyP has peculiar strains within an altered intestinal flora (a condition termed dysbiosis) which contribute most strongly to iPolyP synthesis. However, emerging studies, assisted by state-of-the art methodologies, are revealing the influence of a dysbiotic phenotype in CRC onset and progression, which is bringing to light an exponential number of novel biomarkers [45,46]. In this context we studied whether iPolyP, either of bacterial or human origin, could somehow foster the pathogenesis of CRC. By applying in-vitro and ex-vivo approaches, we demonstrated for the first time that iPolyP facilitates CRC cells proliferation by markedly engaging the TRPM8 receptor channel. This conclusion is based on the following evidence, summarized in Figure 7A: (i) tumoral tissues isolated from CRC subjects betrayed elevated levels of iPolyP, proportional to the amount of the PCNA proliferation marker; (ii) iPolyP governs CRC cell lines proliferation by interacting with the TRPM8 receptor, found to be positively correlated with the concentrations of iPolyP within tumoral tissues; (iii) ex-vivo experiments, performed on CRC patients-derived organoids and in-vitro 3D cell culture, showed a significantly higher growth rate in the presence of iPolyP compared to untreated samples or samples in which TRPM8 was antagonized, (iv) the iPolyP-TRPM8 axis engagement triggers the expression of *ccnb1*, whose corresponding protein product is Cyclin B, which drives the cells into the mitotic phase of the cell cycle. Understanding the source of iPolyP is becoming decisive to target the proliferative pathway. Several studies in the field of microbiology are nowadays focusing on pathogenic bacteria, such as *Salmonella enterica*, with particular emphasis on the mechanism employed by iPolyP in the onset of disparate mammalian diseases [47–49]. Intriguingly, a recent article led by Boyineni and colleagues showed that cancer cells are capable to endogenously produce iPolyP which fosters the metabolism under their period of starvation, as a result of insufficient tumor vascular supply [50]. Thus, ongoing mass spectrometry experiments in our laboratory aim firstly to elucidate the provenience of iPolyP within CRC context, steering research toward the appropriate in-vivo models targeting either the bacterial or human kinase responsible for the inorganic polyphosphate biosynthesis. Although the molecular pathway needs to be fully interpreted, and more experimental evidences are required to confirm our hypothesis, these results uncover a novel, functional axis in the CRC background, shedding light on new directions for study and paving the way for the development of new therapeutic strategies for CRC patients.

 doi:10.20944/preprints202409.0739.v1

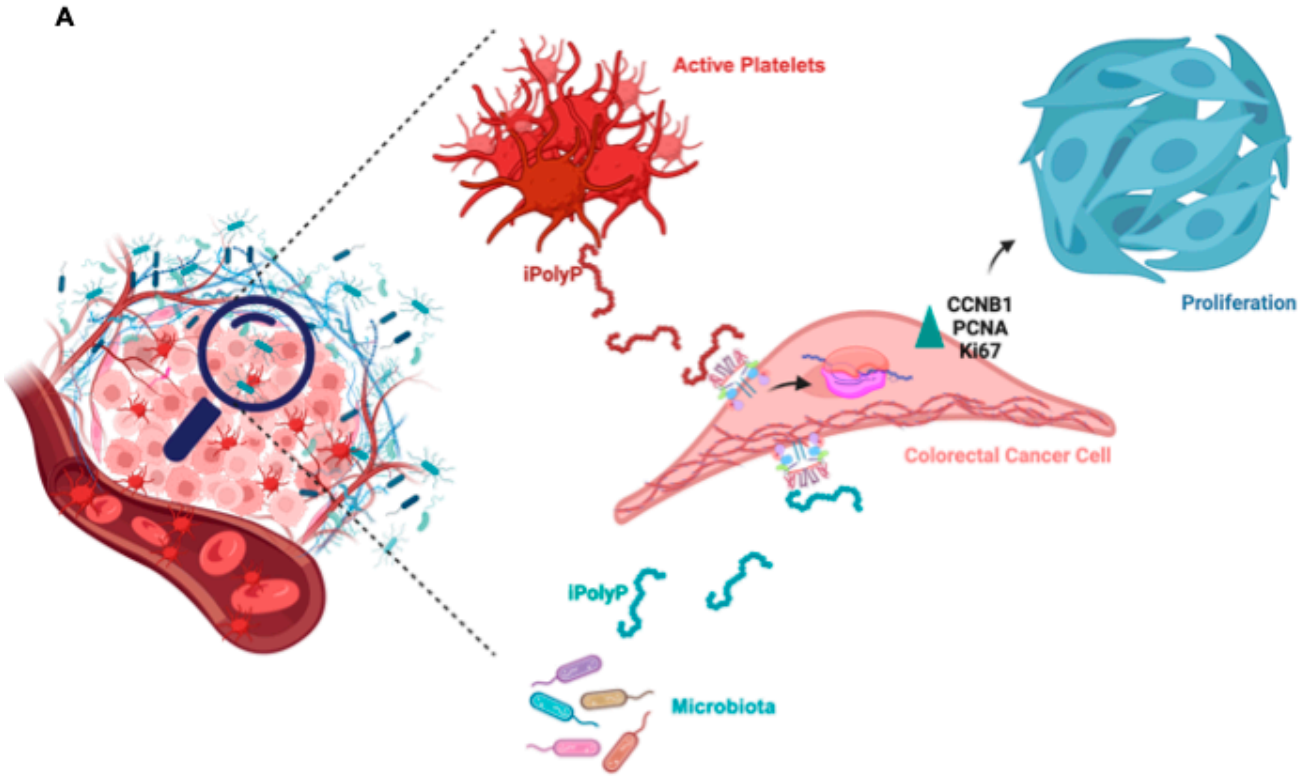

Figure 7. Schematic of the role of iPolyP derived from platelets and microbiota on macrophages and CRC cancer cells. iPolyP-TRPM8 axis stimulates colorectal cancer expansion by enhancing the level of *ccnb1* gene, which coordinates the M phase of the cell cycle, alongside the expression of two *bona fide* proliferative markers, PCNA and Ki67.

5. Conclusions

The findings on the involvement of the iPolyP-TRPM8 axis may offer novel therapeutic options in the fight against CRC, in combination with the conventional chemotherapy protocols applied nowadays. In-vivo experimental models to support our conclusions are currently under study. An early diagnosis of CRC requires a rather invasive method, generally involving biopsy samples taken at certain time intervals. Liquid biopsy offers a valid alternative, without employing invasive procedures, to monitor the disease status, allowing disease detection, and monitoring the progression or response to therapy. Our aim is to test the efficacy of iPolyP as a novel diagnostic and prognostic biomarker to be detected through liquid biopsy or by screening stool samples of CRC-affected subjects.

Supplementary Materials: The following supporting information can be downloaded at the website of this paper posted on Preprints.org. **Supplementary Figure S1. P2Y1 receptor and RAGE receptor level are not altered in CRC**. **A**. Cellular extracts from 4 human biopsies (Patients, Pt), where Tumoral sample (T) was plotted against the Peritumoral (P) counterpart of the same patient, were analyzed by immunoblotting for P2Y1 receptor (P2Y1-R) expression level. Actin was used as loading control for the normalization. **B**. Cellular extracts from 4 human biopsies, where Tumoral sample (T) was plotted against the Peritumoral (P) counterpart of the same patient, were analyzed by immunoblotting for RAGE receptor (RAGE-R) expression level. Actin was used as loading control for the normalization. **Supplementary Figure S2. iPolyP enhances PCNA expression and promotes SW620 colorectal cancer proliferation**. **A**. Cellular extracts from WT and siRNA-mediated TRPM8 knockdown SW620 cell lines were analyzed by immunoblotting for PCNA expression level. GAPDH was used as loading control. **B**. Representative micrographs of the crystal violet assay performed on WT and siRNA-mediated TRPM8 knockdown SW620 cell lines upon treatment for 96 h with iPolyP, TRPM8 inhibitor or both. Scale bar 10 μm. Images are representative of three independent experiments. **C**. Statistical analysis of the crystal violet assay by Student's t-test, respectively for panel **B**, (*** $p < 0.001$ and **** $p < 0.0001$). Fold changes versus control, untreated (UT), normalized to 1. Data are presented as mean ± SD for triplicate wells from three

 doi:10.20944/preprints202409.0739.v1

independent experiments. **Supplementary Figure S3. iPolyP does not compromise HCEC-1CT cell proliferation**. **A**. Cellular extracts from WT and siRNA-mediated TRPM8 knockdown HCEC-1CT cell lines were analyzed by immunoblotting for PCNA expression level. GAPDH was used as loading control. **B**. Representative micrographs of the crystal violet assay performed on WT and siRNA-mediated TRPM8 knockdown HCEC-1CT cell lines upon treatment for 96 h with iPolyP, TRPM8 inhibitor or both. Scale bar 10 μm. Images are representative of three independent experiments. **C**. Statistical analysis of the crystal violet assay by Student's t-test, respectively for panel **B**. Fold changes versus control, untreated (UT), normalized to 1. Data are presented as mean ± SD for triplicate wells from three independent experiments. **Supplementary Figure S4**. **iPolyP does not alter the expression level of RAGE-R or P2Y1-R, not involved in iPolyP-mediated colorectal cancer cellular proliferation**. **A**. Cellular extract from HCEC-1CT, Caco-2 and SW620 cell line were analyzed by immunoblotting for P2Y1-R expression level, with and without iPolyP treatment. GAPDH was used as loading control. **B**. Cellular extract from HCEC-1CT, Caco-2 and SW620 cell line were analyzed by immunoblotting for RAGE-R expression level, with and without iPolyP treatment. GAPDH was used as loading control. **C**. Statistical analysis of the crystal violet assay (data not shown) by Student's t-test, performed with RAGE-R and P2Y1-R inhibitors on Caco-2 cell line and **D**. Statistical analysis of the crystal violet assay (data not shown) by Student's t-test, performed with RAGE-R and P2Y1-R inhibitors on SW620 cell line, (**** $p < 0.0001$); untreated, UT, normalized to 1. Data are presented as mean ± SD for triplicate wells from three independent experiments. **Supplementary Figure S5**. **iPolyP induces nuclear protein Ki-67 expression via TRPM8 in Caco-2 and SW620 cell line**. **A**. Representative immunofluorescence images on WT HCEC-1CT (upper panel), Caco-2 (middle panel) and SW620 (lower panel) cell line and their corresponding siRNA-mediated TRPM8 knockdown, showing the expression of the proliferation marker Ki-67 upon treatment with iPolyP, TRPM8 inhibitor or iPolyP + TRPM8 inhibitor for 72 h. Scale bar 10 μm. Images are representative of three independent experiments. **B**. Fold changes versus control, untreated (UT). Statistical analysis performed by Student's t-test, relative to panel A (** $p < 0.01$, *** $p < 0.001$, **** $p < 0.0001$). Data are presented as mean ± SD for triplicate wells from three independent experiments.

Author Contributions: R.N. and V.A. conceived the project, designed research and supervised the experimental work; V.A., F.B. R.S., F.D., R.D., S.C., D.S., A.B., L.V., S.F. performed the experiments; V.A. C.S., G.P., M.P.S., G.G., R.N. analyzed the data and interpreted the results; V.A., M.P.S., G.G. and R.N. wrote and revised the manuscript. All authors reviewed and approved the manuscript before submission.

Funding: This study was supported by the Ministero della Salute (Italian Minister of Health), Ricerca Corrente 2024.

Institutional Review Board Statement: Not applicable.

Informed Consent Statement: Prot. no. 397/C.E. of 16/09/2020. Local Ethics Committee "Gabriella Serio" IRCCS Istituto Tumori "Giovanni Paolo II", Bari, Italy.

Data availability: All data generated or analyzed during this study are included in this article and Supplementary Materials.

Acknowledgments: We thank Domenico De Rasmo, Anna Signorile and Salvatore Scacco for help with iPolyP quantification in all the subjects analyzed in this manuscript. Figure 5B and Figure 8 in this manuscript were created with BioRender (https://app.biorender.com/).

Conflicts of Interest: The authors declare that they have no competing interests.

References

1. Bray, F.; Ferlay, J.; Soerjomataram, I., Siegel, R.L.; Torre, L.A.; Jemal, A. Global cancer statistics 2018: GLOBOCAN estimates of incidence and mortality worldwide for 36 cancers in 185 countries. *CA Cancer J. Clin.* **2018**, 68, 394–424.
2. Jasperson, K.W.; Tuohy, T.M.; Neklason, D.W.; Burt, R.W. Hereditary and Familial Colon Cancer. *Gastroenterology.* **2010**, 136, 2044–2058.
3. Keum, N.; Giovannucci, E. Global Burden of Colorectal Cancer: Emerging Trends, Risk Factors and Prevention Strategies. *Nat. Rev. Gastroenterol. Hepatol.* **2019**, 16, 713–732.
4. Fearon, E.R. Molecular Genetics of Colorectal Cancer. *Annu. Rev. Pathol.* **2011**, 6:479–507.
5. Schmitt, M.; Greten, F.R. The Inflammatory Pathogenesis of Colorectal Cancer. *Nat. Rev. Immunol.* **2021**, 21, 653–667.
6. Kim, J.; Lee, H.K. Potential Role of the Gut Microbiome In Colorectal Cancer Progression. *Front. Immunol.* **2021**, 12.
7. Hassanian, S.M.; Avan, A.; Ardeshirylajimi, A. Inorganic polyphosphate: a key modulator of inflammation. J. *Thromb. Haemost.* **2017**, 15, 213–218.

8. Kulakovskaya, T.; Pavlov, E.; Dedkova, E.N. Inorganic Polyphosphate in Eukaryotic Cells. 1st ed.; Springer; 2016.
9. Kulakovskaya, E.V.; Zemskova, M.Y.; Kulakovskaya, T.V. Inorganic Polyphosphate and Cancer. *Biochemistry (Mosc).* **2018**, 83, 961–968.
10. Kornberg, A.; Inorganic polyphosphate: toward making a forgotten polymer unforgettable. *J. Bacteriol.* **1995**, 177:491–496.
11. Pisoni, R.L.; Lindley, E.R. Incorporation of [32P]orthophosphate into long chains of inorganic polyphosphate within lysosomes of human fibroblasts. *J. Biol. Chem.* **1992**, 267, 3626–3631.
12. Ruiz, F.A.; Lea, C.R.; Oldfield, E.; Docampo, R. Human platelet dense granules contain polyphosphate and are similar to acidocalcisomes of bacteria and unicellular eukaryotes. *J. Biol. Chem.* **2004**, 44250– 44257.
13. Moreno-Sanchez, D.; Hernandez-Ruiz, L.; Ruiz, F.A.; Docampo, R. Polyphosphate is a novel pro-Inflammatory regulator of mast cells and is located in acidocalcisomes. *J. Biol. Chem.* **2012**, 287, 28435–28444.
14. Müller, W.E.G., Wang, S.; Neufurth, M.; Kokkinopoulou, M.; Feng, Q.; Schröder, H.C.; Wang, X. Polyphosphate as a donor of high-energy phosphate for the synthesis of ADP and ATP. *J. Cell. Sci.* **2017**, 130, 2747-2756.
15. Bae, J.-S., Lee, W., Rezaie, A.R. Polyphosphate elicits pro-inflammatory responses that are counteracted By activated protein C in both cellular and animal models. *J. Thromb. Haemost.* **2012**, 10, 1145–1151.
16. Müller, F.; Mutch, N.J.; Schenk, W.A.; Smith, S.A.; Esterl, L.; Spronk, H.M.; Schmidbauer, S.; Gahl, W.A.; Morrissey, J.H.; Renné T. Platelet polyphosphates are proinflammatory and procoagulant mediators in vivo. *Cell*. **2009**,139, 1143–1456.
17. Hassanian, S.M.; Dinarvand, P.; Smith, S.A.; Rezaie, A.R. Inorganic polyphosphate elicits pro-inflammatory responses through activation of the mammalian target of rapamycin complexes 1 and 2 in vascular endothelial cells. *J. Thromb. Haemost.* **2015**, 860–871.
18. Semeraro, F.; Ammollo, C.T.; Morrissey, J.H.; Dale, G.L.; Friese, P.; Esmon, N.L.; Esmon, C.T. Extracellular histones promote thrombin generation through platelet-dependent mechanisms: involvement of platelet TLR2 and TLR4. *Blood*. **2011**, 118, 1952–1961.
19. Wat, J.M.; Foley, J.H.; Krisinger, M.J.; Ocariza, L.M.; Lei, V.; Wasney, G.A.; Lameignere, E.; Strynadka, N.C.; Smith S.A.; Morrissey, J.H. et al. Polyphosphate suppresses complement via the terminal pathway. *Blood*. **2014**, 123, 768–776.
20. Wijeyewickrema, L.C.; Lameignere, E., Hor, L.; Duncan, R.C.; Shiba, T., Travers, R.J., Kapopara P.R.; Lei, V.; Smith, S.A.; Kim. H.; et al. Polyphosphate is a novel cofactor for regulation of complement by a serpin, C1 inhibitor. *Blood*. **2016**, 128, 1766–1776.
21. Galasso, A.; Zollo, M. The Nm23-H1-h-Prune complex in cellular physiology: a 'tip of the iceberg' protein network perspective. *Mol. Cell. Biochem.* **2009**, 329, 149–159.
22. Tammenkoski, M.; Koivula, K.; Cusanelli, E.; Zollo, M.; Steegborn, C.; Baykov, A.A.; Lahti, R. Human metastasis regulator protein H-prune is a short-chain exopolyphosphatase. *Biochemistry.* **2008**, 47, 9707–9713.
23. Wang, L.; Fraley, C.D.; Faridi, J.; Kornberg, A.; Roth, R.A. Inorganic polyphosphate stimulates mammalian TOR, a kinase involved in the proliferation of mammary cancer cells. *Proc. Natl. Acad. Sci. U S A.* **2003**, 100,11249–12254.
24. Ito, T., Yamamoto, S.; Yamaguchi, K.; Sato, M.; Kaneko, Y.; Goto, S.; Goto Y., Narita, I. Inorganic polyphosphate potentiates lipopolysaccharide-induced macrophage inflammatory response. *J. Biol. Chem.* **2020**, 295, 4014–4023.
25. Dinarvand, P.; Hassanian, S.M.; Qureshi, S.H.; Manithody, C.; Eissenberg, J.C.; Yang, L., Rezaie, A.R. Polyphosphate amplifies proinflammatory responses of nuclear proteins through interaction with receptor. for advanced glycation end products and P2Y1 purinergic receptor. *Blood*. **2014**, 123, 935–945.
26. Zakharian, E.; Thyagarajan, B.; French, R.J.; Pavlov, E.; Rohacs, T. Inorganic polyphosphate modulates TRPM8 Channels. *PLoS One*. **2009**, 4, e5404.
27. Hassanian, S.M., Ardeshirylajimi, A, Dinarvand, P, Rezaie, AR. Inorganic polyphosphate promotes cyclin D1 synthesis through activation of mTOR/Wnt/β-catenin signaling in endothelial cells. *J. Thromb. Haemost.* **2016**, 14, 2261-2273.
28. Tsutsumi, K.; Tippayamontri, T.; Hayashi, M.; Matsuda, N.; Goto, Y. The dynamic relationship between inorganic polyphosphate and adenosine triphosphate in human non-small cell lung cancer H1299 cells. *FEBS Open Bio*. **2024**, 14, 344–354.
29. Pagano, P.; Romano, B.; Cicia, D.; Iannotti, F.A.; Venneri, T.; Lucariello, G.; Nanì, M.F.; Cattaneo, F.; De Cicco, P.; D'Armiento, M.; et al. TRPM8 indicates poor prognosis in colorectal cancer patients and its pharmacological targeting reduces tumour growth in mice by inhibiting Wnt/β-catenin signalling. *Br. J. Pharmacol.* **2023**, 180, 235-251.
30. Yin, Y.; Zhang, F.; Feng, S.; Butay, K.J.; Borgnia, M.J.; Im, W.; Lee S.-Y. Activation mechanism of the mouse cold-sensing TRPM8 channel by cooling agonist and PIP2. *Science*. **2022**, 378, eadd1268.

31. Ogunwobi, O.O.; Mahmood, F.; Akingboye, A. Biomarkers in Colorectal Cancer: Current Research and Future Prospects. *Int. J. Mol. Sci.* **2020**, 21, 5311.
32. Vlachogiannis, G.; Hedayat, S.; Vatsiou A.; Jamin. Y.; Fernández-Mateos, J.; Khan, K.; Lampis, A, Eason, K.; Huntingford, I.; Burke, R.; et al. Patient-derived organoids model treatment response of metastatic gastrointestinal cancers. *Science.* **2018**, 359, 920–926.
33. Hossain, M.S.; Karuniawati, H.; Jairoun, A.A.; Urbi, Z., Ooi, D.J.; John, A.; Lim, Y.C.; Kibria, K.M.K.; Mohiuddin, A.K.M.; Ming, L.C.; et al. Colorectal Cancer: A Review of Carcinogenesis, Global Epidemiology, Current Challenges, Risk Factors, Preventive and Treatment Strategies. *Cancers (Basel).* **2022**, 14,1732.
34. Hibberd, A.A.; Lyra, A.; Ouwehand, A.C.; Rolny, P.; Lindegren, H.; Cedgård, L.; Wettergren, Y. Intestinal microbiota is altered in patients with colon cancer and modified by probiotic intervention. *BMJ Open Gastroenterol.* **2017**, 4, e000145.
35. Zackular, J.P.; Baxter, N.T.; Iverson, K.D.; Sadler, W.D.; Petrosino, J.F.; Chen, G.Y.; Schloss, P.D. The gut microbiome modulates colon tumorigenesis. *mBio.* **2013**, 4, e00692-13.
36. Karaca, C.; Karaman, E.D.; Leblebici, A.; Kurter, H.; Ellidokuz, H.; Koc, A.; Ellidokuz, E.B.; Isik, Z.; Basbinar, Y. New treatment alternatives for primary and metastatic colorectal cancer by an integrated transcriptome and network analyses. *Sci. Rep.* **2024**, 14, 8762.
37. Wu, Z.; Zuo, M.; Zeng, L.; Cui, K.; Liu, B.; Yan, C.; Chen, L.; Dong, J.; Shangguan, F.; Hu, W., et al. OMA1 reprograms metabolism under hypoxia to promote colorectal cancer development. *EMBO Rep.* **2021**; 22, e50827.
38. Rao, N.N.; Gómez-García, M.R.; Kornberg, A. Inorganic polyphosphate: essential for growth and survival. *Annu. Rev. Biochem.* **2009**, 78, 605–647.
39. Kornberg, A.; Rao, N.N. Ault-Riché D. Inorganic polyphosphate: a molecule of many functions. *Annu. Rev. Biochem.* **1999**, 68, 89–125.
40. Kumble, K.D.; Kornberg, A. Inorganic polyphosphate in mammalian cells and tissues. *J. Biol. Chem.* **1995**, 70, 5818–5822.
41. Ahn, K.; Kornberg, A. Polyphosphate kinase from Escherichia coli. Purification and demonstration of a phosphoenzyme intermediate. *J. Biol. Chem.* **1990**, 265(20):11734–11739.
42. Schröder, H.C.; Kurz, L.; Müller, W.E. Lorenz, B. Polyphosphate in bone. *Biochemistry (Mosc).* **2000**, 65(3):296–303.
43. Müller, F.; Mutch, N.J.; Schenk, W.A.; Smith, S.A.; Esterl, L.; Spronk, H.M., et al. Platelet polyphosphates are proinflammatory and procoagulant mediators in vivo. *Cell.* **2009**, 139, 1143–1156.
44. Docampo R. Polyphosphate: a target for thrombosis attenuation. *Blood.* **2014**, 124, 3177–3178.
45. Dulal, S.; Keku, T.O. Gut microbiome and colorectal adenomas. *Cancer J.* **2014**, 20(3):225–231.
46. Flemer, B.; Lynch, C.B.; Brown, J.M.R.; Jeffery, I.B.; Ryan, F.J.; Claesson, M.J.; O'Riordain M.; Shanahan F.; O'Toole, P.W.l. Tumour-associated and non-tumour-associated microbiota in colorectal cancer. *Gut*. **2017**, 66, 633–643.
47. Candon, H.L.; Allan, B.J.; Fraley, C.D.; Gaynor, E.C. Polyphosphate kinase 1 is a pathogenesis determinant in Campylobacter jejuni. *J. Bacteriol.* **2007**, 189, 8099-8108.
48. Jenal, U.; Hengge-Aronis, R. Regulation by proteolysis in bacterial cells. *Curr. Opin. Microbiol.* **2003**, 6, 163-172.
49. Bowlin, M.Q.; Gray, M.J. Inorganic Polyphosphate in Host and Microbe Biology. *Trends Microbiol.* **2021**; 29, 1013–1023.
50. Boyineni, J.; Sredni, S.T., Margaryan, N.V.; Demirkhanyan, L.; Tye, M.; Johnson, R.; Gonzalez-Nilo, F.; Hendrix, M.J.C.; Pavlov, E.; Soares, M.B.; et al. Inorganic polyphosphate as an energy source in Tumorigenesis. *Oncotarget.* **2020**;11, 4613-4624. B